Surface & Coatings Technology 203 (2008) 317–323

Contents lists available at ScienceDirect

Surface & Coatings Technology

journal homepage: www.elsevier.com/locate/surfcoat

Structures and characteristics of Cr(III)-based conversion coatings on electrogalvanized steels

Niann-Tsyr Wen [a], Chao-Sung Lin [b], Ching-Yuan Bai [c], Ming-Der Ger [c,*]

[a] Graduate School of Defense Science, Chung Cheng Institute of Technology, National Defense University, Tao-Yuan 335, Taiwan, ROC
[b] Department of Materials Science and Engineering, National Taiwan University Taipei 106, Taiwan, ROC
[c] Department of Applied Chemistry & Materials Science, Chung Cheng Institute of Technology, National Defense University, Tao-Yuan 335, Taiwan, ROC

ARTICLE INFO

Article history:
Received 28 March 2008
Accepted in revised form 5 September 2008
Available online 14 September 2008

Keywords:
Electrogalvanized
Trivalent chromium conversion coating
Anions effect
Structure

ABSTRACT

Trivalent chromium (Cr(III)) conversion coatings have been made on electrogalvanized steels in the solutions containing Cr(III) sulfate, nitrate, and chloride among which the sulfate, nitrate, and chloride anions function as passivating, oxidizing, and pitting agents, respectively. The structure and properties of the Cr(III) conversion coatings were examined by electrochemical methods and surface morphology observations. Experimental results showed that the Cr(III) coating formed in the sulfate bath displayed a thin, compact, single-layered structure, before and after baking. The conversion coating formed in the nitrate bath consisted of two porous layers for both the as-deposited and baked states. Moreover, the coating prepared in the chloride bath exhibited a porous, single-layered structure regardless of the baking treatment. Electrochemical impedance analyses further showed that the anions in the bath strongly influenced the structure and corrosion resistances of the Cr(III) coatings.

1. Introduction

Conventional chromate conversion coating (CCC) has superior corrosion resistance and self-healing ability. However, the CCC treatment employs hexavalent chromium ions, Cr(VI), whose use has been limited by several environmental legislations. This is because Cr(VI) displays high toxicity for human health and causes serious environmental pollutions. On the contrary, trivalent chromium, Cr(III), has low toxicity, and the wastewater and solid waste from the Cr(III) bath can be treated in a simple and efficient way. Moreover, the industrial implementation of Cr(III) conversion coating is similar to that of the chromate counterpart. Hence, the Cr(III) conversion coating treatment is one of the potential alternatives to the CCC process for zinc-coated steels [1–7].

In general, the formation of cracks deteriorates the corrosion resistance of the conversion coating. Gigandet et al. [8] and Cho et al. [4] observed that cracks form in CCCs during the immersion in the solution or the baking process. However, the CCCs have self-healing capability to repair themselves at defect sites and maintain an excellent corrosion resistance. Conversely, other metallic ions (including Cr(III)) in conversion coatings lack the capability to heal coating defects. Therefore, developing a conversion coating process to replace the CCCs progresses at a slow pace, and how to reduce the density of cracks will be the key point to impart non-chromate conversion coatings with adequate corrosion protection properties.

Electrochemical impedance spectroscopy (EIS) has long been used to estimate the corrosion resistance of functional coatings. EIS is a very outstanding tool widely employed in the study of conversion coatings, because it can be used to elucidate the coating structure via simulating the EIS data using a proper equivalent circuit. For example, Tan et al. studied the inhibiting carbon dioxide corrosion afforded by imidazoline, and demonstrated that the imidazoline film had a four-layer structure as seen in EIS equivalent circuits [9]. Zheludkevich et al. investigated the anticorrosion performance of Al alloy AA2024-T3 pre-treated with cerium nitrate, and identified the transformation of the Al alloy surface structures after corroding using the equivalent circuit [10]. Moreover, Cho et al. reported that the crack form of the Cr(III) conversion coating can be explained by modified equivalent circuits with a Warburg diffusion element [4]. In general, the EIS impedance plots are not enough to directly analyze the conversion coatings with complicated structures. Nevertheless, it is convenient and competent that using the equivalent circuit to evaluate the structure and corrosion resistance of conversion coatings.

This work studied the characteristics of the conversion coatings on electrogalvanized steels in Cr(III)-based solutions with the emphasis on the effect of anions. At first, the open circuit potential (OCP) method was used to analyze the potential change as immersion proceeded. The structure and morphology of the coatings was observed by field-emission scanning electron microscope (FE-SEM). Finally, the EIS impedance plots and equivalent circuits were employed to evaluate the properties and construct the structures of these coatings.

* Corresponding author. Tel.: +886 3 3891716; fax: +886 3 3892494.
E-mail address: mdger@ccit.edu.tw (M.-D. Ger).

0257-8972/$ – see front matter © 2008 Elsevier B.V. All rights reserved.
doi:10.1016/j.surfcoat.2008.09.006

2. Experiments

2.1. Conversion coating treatment

Cr(III)-based solutions were prepared using reagent-grade Cr(III) sulfate, nitrate, and chloride. The concentration ratio of Cr(III) to the various anions was set to be 1/3, which the [Cr(III)] was 0.1 M. The Cr (III)-based aqueous solutions were heated and stirred at 80 °C for 4 h, adjusted to pH 2, and then kept stable for 24 h before use for the conversion coating treatment. For the sulfate bath, additional sulfate ions were added as sodium sulfate. Prior to the conversion coating treatment, electrogalvanized steel plates were activated in a 0.5% v/v nitric acid solution for 10 s, and thoroughly rinsed in running deionized water. These plates were immersed in different Cr(III)-based solutions at 60 °C for 60 s, rinsed in deionized water, and then dried by compressed air. After immersion, the plates were either left for drying at room temperature air or baked in 90 °C air for 90 min. The Cr(III) coating prepared in the sulfate, nitrate, and chloride bath, was denoted as TCS, TCN, and TCC, respectively. The corresponding specimen subjected to the baking treatment was, accordingly, denoted as TCSH, TCNH, and TCCH.

2.2. Electrochemical analyses and microstructural investigations

All electrochemical experiments were carried out in a three-electrode cell system, in which platinum sheet and Ag/AgCl electrode (197 mV versus SHE) were used as the counter and reference electrodes, respectively. The working electrode was an electrogalvanized steel plate and the electrolytes were the Cr(III)-based solutions for the open circuit potential (OCP) measurement, which was carried out to record the mixing potential versus reaction time (E_{ocp} vs. time).

Electrochemical impedance spectroscopy (EIS) measurement was conducted in a 3.5 wt.% sodium chloride solution, in which the working electrode was the electrogalvanized steel with Cr(III) coatings. Each EIS spectrum was recorded at corrosion potential (E_{corr}) in frequencies ranging from 10^5~10^{-2} Hz, with a sinusoidal signal amplitude of 10 mV, to construct the Nyquist and Bode plots and the equivalent circuit. The OCP and EIS measurements were performed using an Autolab PGSTAT30 potentiostat/galvanostat controlled by GPES (General Purpose Electrochemical System) and FRA (Frequency Response Analyzer) software.

Finally, the structure, surface morphology, and composition of the Cr(III) coatings in both as-deposited and baked states were investigated using field-emission scanning electron microscopy (FE-SEM; JEOL JSM-6500F) and X-ray photoelectron spectrometry (XPS; ULVAC-PHI XPS).

3. Results and discussion

3.1. OCP measurements

To produce conversion coatings in aqueous solutions, both oxidation and reduction reactions should simultaneously occur in an electrical double layer, the interface between the electrolyte and the electrode. The redox reactions, including the anode, cathode, adsorption, and desorption reactions, are complicated and hard to distinguish. However, the mixed potential of these reactions can be measured by the method of OCP [11]. The OCP data are commonly recorded and shown by the potential as a function of the reaction time.

Fig. 1(a)–(c) shows OCP curves of the electrogalvanized steels in the baths containing Cr(III) sulfate, nitrate, and chloride, respectively. Apparently, each curve comprised two stages, i.e. unsteady and steady states, in the evolution of OCP with time. At the unsteady state or transient stage, the mixed potential (E_{ocp}) evidently changed with the reaction time, revealing that the formation of the Cr(III) conversion

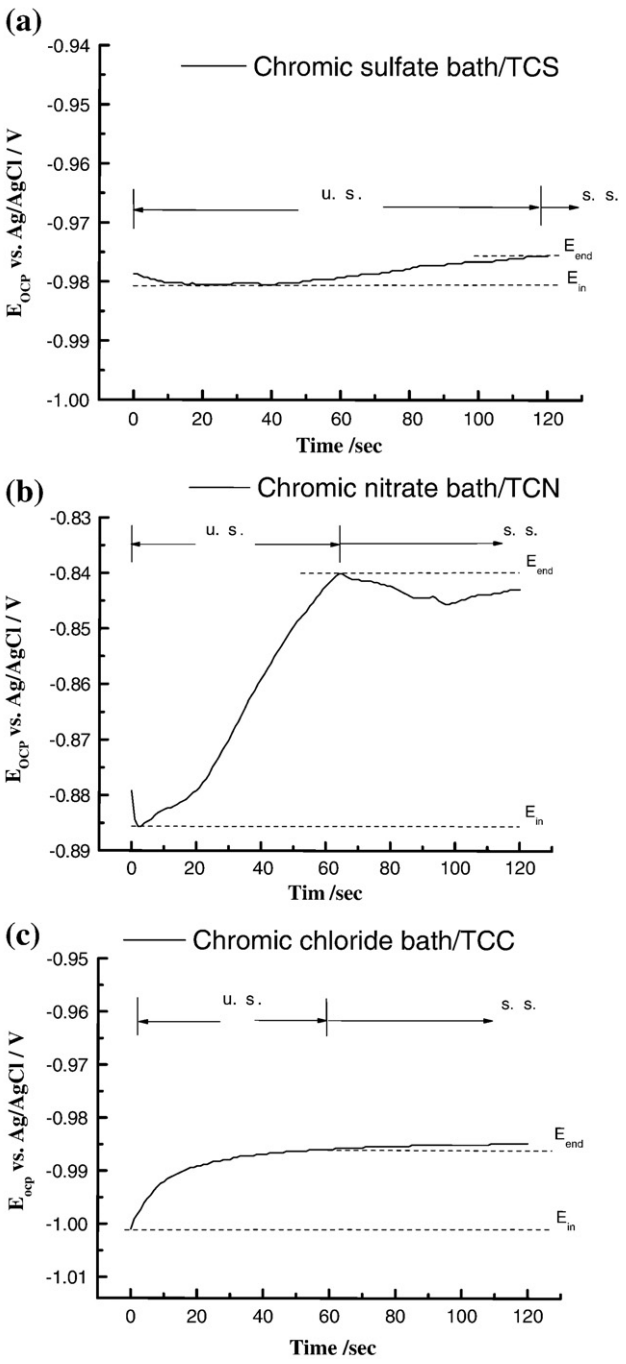

Fig. 1. OCP curves of electrogalvanized steels immersed in the baths containing Cr(III) (a) sulfate, (b) nitrate, and (c) chloride.

coating on electrogalvanized steels proceeded mainly at such stage. In contrast, the mixed potential changed insignificantly with continued immersion at the steady-state stage. At this stage, the mixed potential represented the surface potential of the Cr(III) conversion coating, $E_{coating}$. To analyze the OCP curves of Cr(III) conversion coatings, the difference between the initial potential (E_{in}) and final potential (E_{end}) at the unsteady state stage was herein defined as $\Delta E = E_{end} - E_{in}$, and named as the formation potential. The reaction time at the same stage was accordingly named as the formation time, Δt. The ΔE and Δt can be used to evaluate the driving force and the proceeding period, respectively, of the coating formation in the different baths.

E_{in}, E_{end}, ΔE, Δt, and $E_{coating}$, acquired by analyzing the OCP curves in the three Cr(III)-based solutions are listed in Table 1. The ranking of

Table 1
Various OCP measurement parameters of Cr(III) conversion coatings

Cr(III) baths	Initial potential E_{in} (V)	Final potential E_{end} (V)	Forming potential ΔE (V)	Forming time Δt (s)	Coating surface potential $E_{coating}$ (V)
$Cr_2(SO_4)_3$	−0.981	−0.975	0.006	120	−0.975
$Cr(NO_3)_3$	−0.886	−0.840	0.044	62	−0.840
$CrCl_3$	−1.000	−0.986	0.014	60	−0.986

Ag/AgCl reference electrode.

E_{in} measured in the different baths was in order the nitrate, sulfate, and chloride bath. This indicates that the chloride bath is the most active one for the electrogalvanized steels. Additionally, the sequence of ΔE, from the large to the small, was as follows: the nitrate bath, chloride bath, and sulfate bath. Therefore, the driving force for the formation of the Cr(III) coating on electrogalvanized steels was largest in the nitrate bath; whereas, the driving force in the sulfate bath was lowest. The order of $E_{coating}$, from the large to the small, was as follows: TCN, TCS, and TCC, suggesting that the TCN was the most passive among the three conversion coatings. Moreover, the Δt of the Cr(III) conversion coatings, listed in Table 1, were different for dissimilar baths. Nevertheless, the treating time of the conversion specimens was taken as 60 s in three different baths for comparing the characteristics of conversion coatings in the same criterion.

3.2. Surface morphology of the conversion coating

Cr(III) ions usually exist in the form of chromic salts, which are composed of Cr(III) ions and anions such as sulfate, nitrate, and chloride. It is interesting to note that the sulfate, nitrate, and chloride ions in the Cr(III)-based solutions investigated in this present study potentially act as the passivating [12], oxidizing [13], and pitting [14] agents, respectively. Therefore, the anions in the bath can markedly influence the morphology and properties of the Cr(III) coatings.

Fig. 2(a)–(c) shows the SEM surface morphology of the as-deposited Cr(III) conversion coating, TCS, TCN, and TCC, respectively.

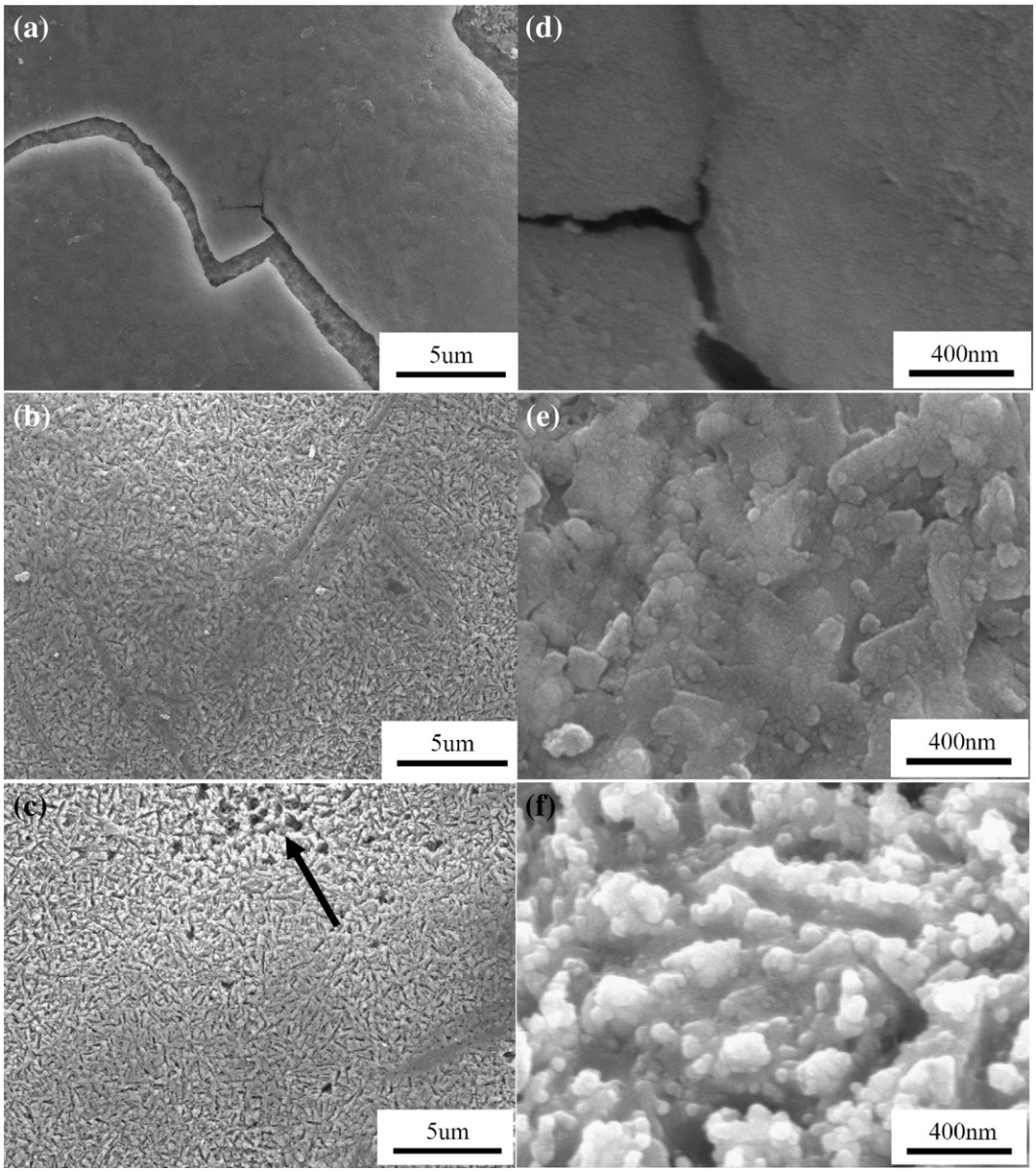

Fig. 2. SEM micrographs of the as-plated Cr(III) coatings: (a) TCS, (b) TCN, and (c) TCC specimens(×500), and (d), (e), and (f) are the magnified view(×60,000) of (a), (b), and (c), respectively.

Table 2
The composition of various Cr(III) conversion coatings determined by XPS analysis

Coatings	Atomic %					
	Zn	O	Cr	S	N	Cl
TCS	20.24	53.14	23.25	2.37		
TCN	31.61	43.22	23.25		1.92	
TCC	31.40	37.17	30.10			1.34
TCSH	15.79	52.96	26.58	4.67		
TCNH	20.90	51.01	26.37		1.71	
TCCH	29.92	41.42	27.92			0.75

These coatings were prepared in the baths with 0.1 M Cr(III) at pH 2 and 60 °C for 60 s. The TCS specimen (Fig. 2(a) and (d)) displayed a very smooth and dense surface morphology without pores, despite the presence of crevices. These crevices are likely to be due to the dehydration of the coating after the specimen was removed from the solution, but was absent during immersion. Therefore, the amounts of defects or diffusion channels in the TCS coating are inadequate for the solution to penetrate to the coating/substrate interface. The growth of the TCS film was, thus, retarded due to the insufficient reaction species at the interface between the coating and the substrate. On the contrary, the surface morphology of the TCN and TCC coatings (Fig. 2 (b) and (c)) showed, respectively, a porous structure with numerous microvoids and a dendritic structure with several large holes. There are many penetration paths for the reaction species in these films, and the conversion agents are abundant for the growth of the conversion coating at the coating/substrate interface. Moreover, the chloride ions in the solution caused the pitting corrosion in the Cr(III) coating, and the evident by the presence of large voids in Fig. 2(c) (indicated by the arrows). The different SEM superficial appearance of the conversion coatings were mainly caused by the use of different treatment solutions, which contain special anions such as sulfate, nitrate, and chloride. The correlation between the OCP and the morphology of the conversion coatings is indirect, although the structure analyses are in agreement with the ΔE results of the coatings in the OCP measurement.

Table 2 shows the average atomic compositions, determined by XPS analysis, of various Cr(III) conversion coatings. It revealed that the

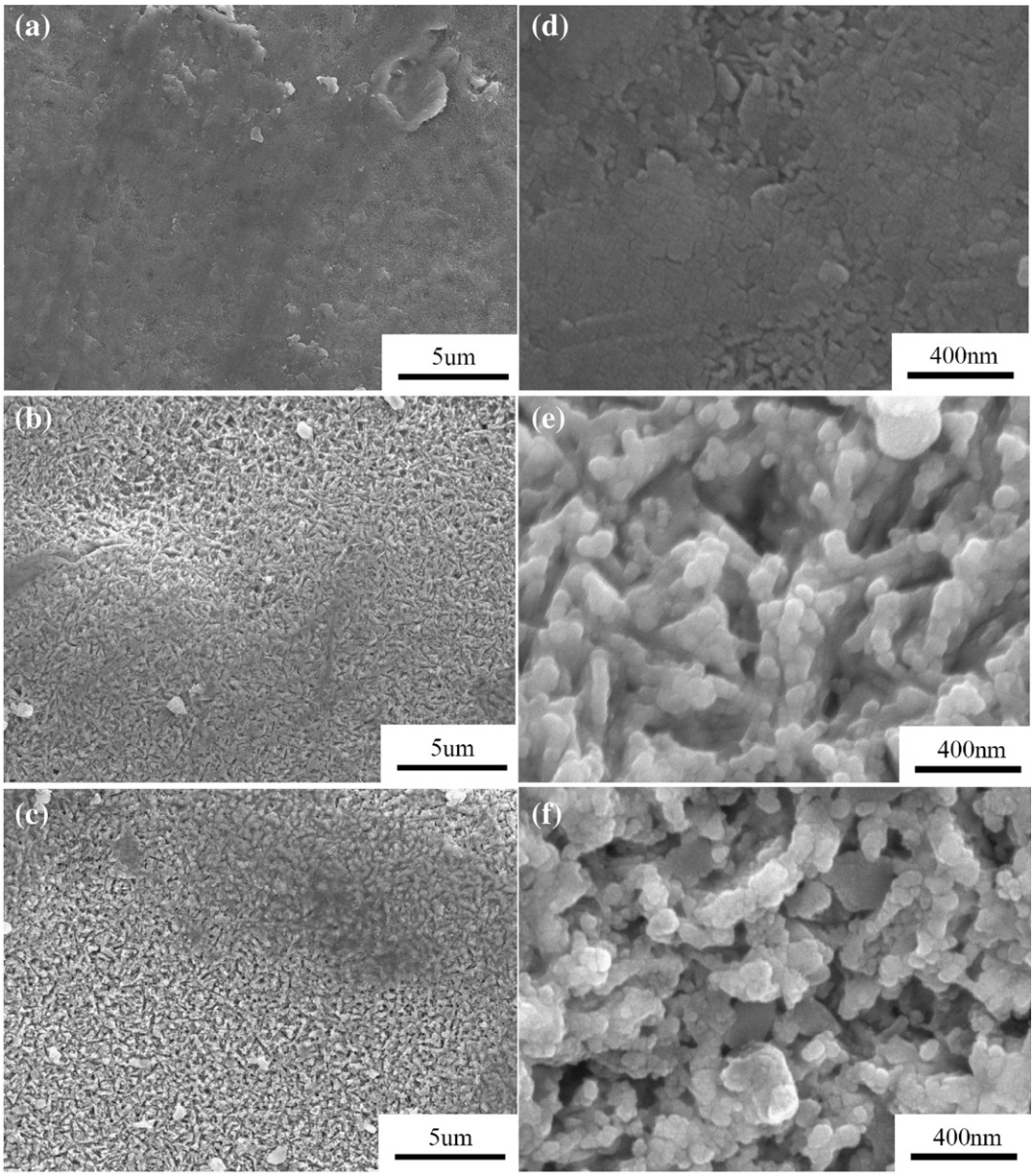

Fig. 3. SEM micrographs of the baked Cr(III) coatings: (a) TCSH, (b) TCNH, (c) TCCH specimens (×500), (d), (e), and (f) are the magnified view (×60,000) of (a), (b), and (c), respectively.

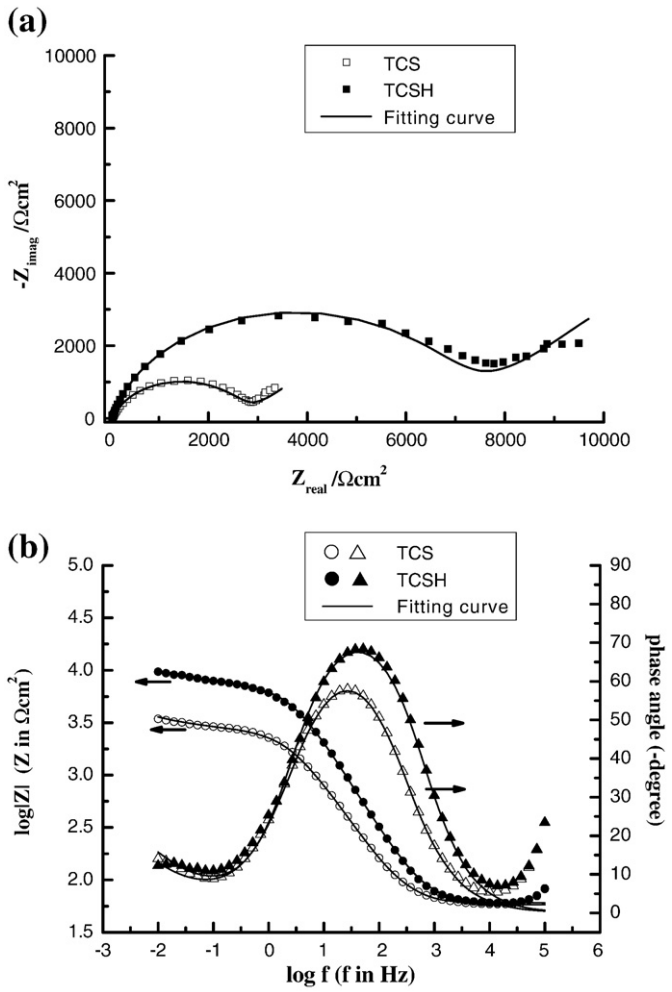

Fig. 4. (a) Nyquist and (b) Bode plots of the TCS and TCSH specimens.

coatings were substantially composed of Cr, Zn, O, and some corresponding acidic elements.

Fig. 3(a)–(c) shows the SEM micrographs of the conversion coatings after baking, i.e. TCSH, TCNH, and TCCH, and the corresponding enlarged images for each specimen are presented in Fig. 3(d)–(f). The TCSH film exhibited a dense surface morphology that is similar to the surface condition of the as-deposited TCS film. The overall appearance of the TCNH film was more porous and uneven than that of the TCN coating. The surface morphology of the TCCH resembled that of the TCC, however, the pitting holes in the as-deposited TCC coating disappeared after baking. Furthermore, the surface condition of the Cr(III) conversion coatings changed apparently, as shown by comparing the as-deposited and baked coatings. It is likely that the coating constituents changed due to the dehydration reaction during baking. Gigandet et al. [8] proposed that hydroxides in chromate conversion coatings can transform to oxides by dehydration reaction during the baking treatment. Moreover, Gigandet et al. [8] and Cho et al. [4] reported that the baking treatment induced many cracks by releasing the internal stresses of the as-deposited conversion coatings. In this present study, the density of cracks did not increase after baking. To enhance the corrosion resistance of the Cr(III) coatings, their crack density should be reduced as far as possible because they are lack of self-healing capability. The Cr(III) conversion coatings studied in this work have a porous structure whose porosity depends on the anions in the solution. Therefore, it can be expected that the corrosion resistance of the Cr(III) conversion coating can be enhanced by reducing the porosity and crack density of the coating formed in the solution with specific anions.

3.3. EIS analyses

Figs. 4–6 show the Nyquist and Bode plots of the as-deposited and baked Cr(III) conversion coatings prepared in the sulfate, nitrate, and chloride baths, respectively. The electrochemical impedance spectra reveal that the characteristics of the various Cr(III) conversion baths were different, and the Nyquist plots show that the impedance of all the Cr(III) coatings was composed of the coating resistance and the diffusion effect. However, modeling the impedance data using an equivalent circuit is necessary to explicate the difference in the structure and corrosion resistance of the various Cr(III) conversion coatings before and after the baking treatment.

In general, the constant phase element (CPE) and the diffusion elements are the main components used to construct the equivalent circuit of the conversion coatings. These two components can respond the potential perturbation in the conversion coating system. A conversion coating may consist of several heterogeneous layers. One heterogeneous layer can be expressed as a parallel circuit containing two branches in an equivalent circuit: a nonideal capacitance (Q), and a resistance (R). The nonideal capacitance is called the constant phase element. Therefore, the equivalent circuit of a conversion film including n heterogeneous layers would contain n parallel CPEs. This principle has been wildly applied to create the equivalent circuit of the conversion coatings by many researchers [4,9,10,15–19]. For the diffusion element in the equivalent circuit, Jacobsen and West [16] recommended three mathematical models of the diffusion impedance associated with different boundary conditions: Warburg (W),

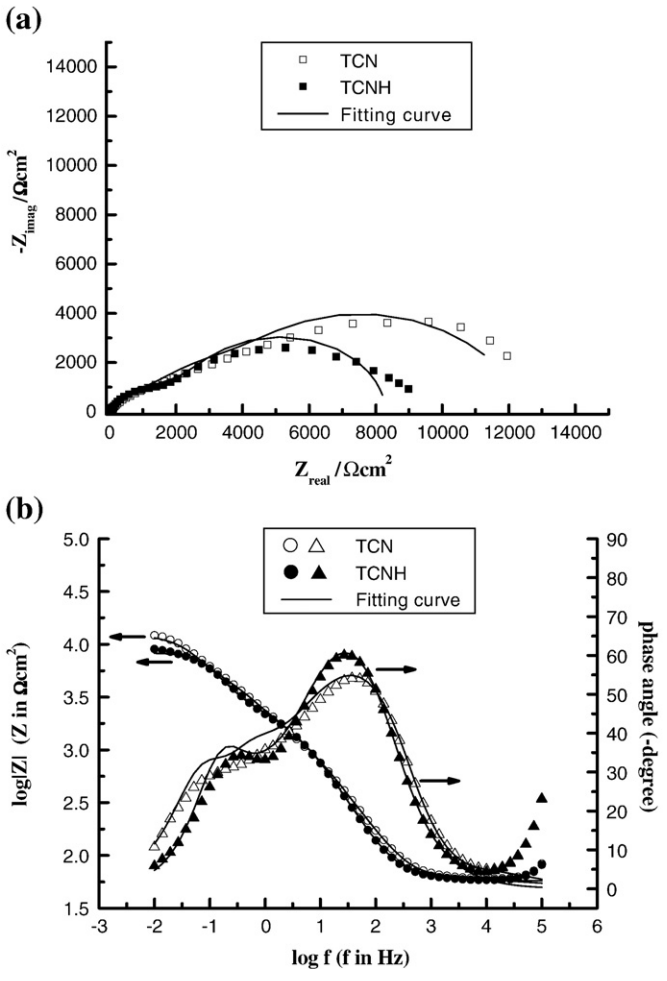

Fig. 5. (a) Nyquist and (b) Bode plots of the TCN and TCNH specimens.

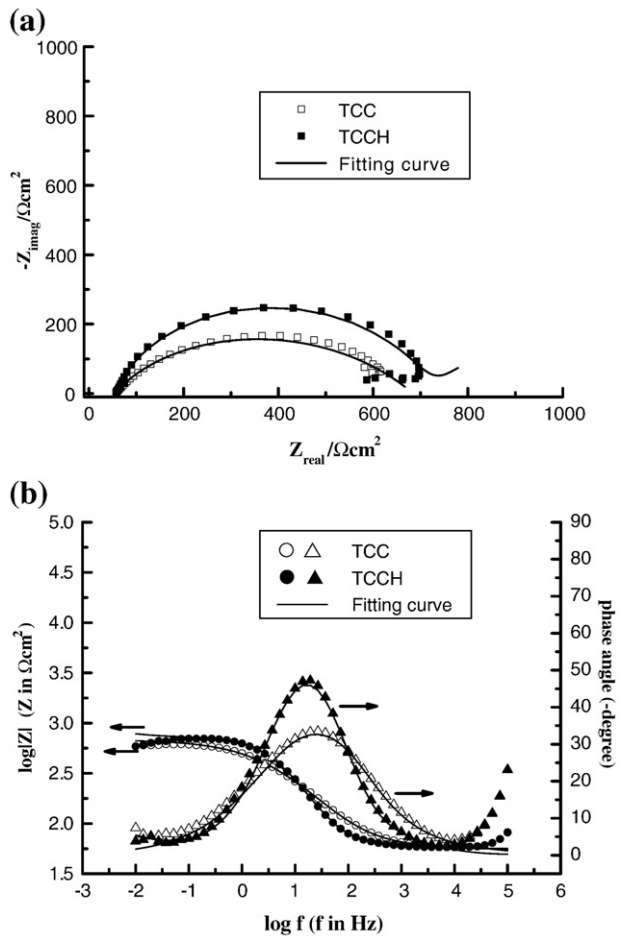

Fig. 6. (a) Nyquist and (b) Bode plots of the TCC and TCCH specimens.

Nernstian (W_O), and Impermeable (W_T) diffusion models, in which the Warburg impedance element (W) can be used to model semi-infinite linear diffusion.

According to the arrangement of CPEs and the evaluation of diffusion models in the EIS equivalent circuits, the structure and character of porous films can be extrapolated. In this study, three modified equivalent circuits were employed to fit the EIS data of the Cr(III) conversion coatings prepared in the various baths, as shown in Fig. 7. In this figure, R_s stands for the electrolyte resistance. Q_n and R_n (n=1–2) are constant phase angle elements and resistive responses, respectively, of the nth layer of Cr(III) conversion coatings. C_{dl} and R_{ct} represent, respectively, the electrical double layer capacitance and charge transfer resistance. W and W_O denote the Warburg impedance and Nernstian diffusion elements, respectively. In addition, R_P ($=R_1+R_2+R_{ct}$) is the total polarization resistance of the coating.

The sketches and equivalent circuits of TCS and TCSH are shown in Fig. 7(a). The circuits of both the as-deposited and baked coatings include a CPE and a Warburg impedance element. It can be seen that the TCS and TCSH coatings had a dense and one-layer structure. Moreover, the R_P value of TCSH was larger than that of TCS, indicating that the integrity of the coating formed in the sulfate bath was enhanced by the baking treatment. Fig. 7(b) represents the sketches and equivalent circuits of TCN and TCNH. Two CPEs and one Nernstian diffusion element, W_O, are drawn in the circuit for both TCN and TCNH coatings to well fit their impedance data. This suggests that both TCN and TCNH coatings were made up of two layers, i.e. outer and inner layers. For the as-deposited coatings, voids in the inner layer were large, and the electrolyte would penetrate through the inner layer. As a result, the diffusion mainly occurred in the electrical double layer, an interface between the inner layer and the substrate. After baking, the inner layer of the coating may shrink with the formation of smaller voids, hence, the diffusion would mostly take place in the inner layer of the TCNH coating. The equivalent circuits of both TCC and TCCH coatings (Fig. 7(c)) comprise a CPE and a diffusion element, demonstrating that both TCC and TCCH had a one-layer structure. The diffusion behavior of reaction species in the TCC coating is suitable to be described by the Nernstian model, but this model is inappropriate to be employed for the TCCH coating. The diffusion behavior of electrolytes has to be illustrated by the Warburg diffusion model for well fitting impedance data of the TCCH coating, and then a very large admittance constant (Y_0), about 86,760 $\mu s^{0.5}\ \Omega^{-1}\ cm^{-2}$, was obtained in the diffusion element. The large value of Y_0 suggests that the baking treatment may enhance the solution permeability of the coating.

The various electrical parameters, obtained from the EIS simulations, of the as-deposited and the baked Cr(III) conversion coatings are listed in Table 3. The R_P of TCN, calculated from the equivalent circuit, was about 4.47 kΩ cm^2, nevertheless, that measured in the Nyquist plot was approximately 12 kΩ cm^2. It is likely that diffusion behaviors occurring in the conversion coating may cause the increment of R_P in Nyquist results [17,20]. Therefore, it is necessary to determine a correct R_P of a specific coating by using proper equivalent circuits. As can be seen in Figs. 4, 5, and 6, the impedance data can be well fit, marked by the solid lines, using the present modified equivalent circuits. Consequently, these equivalent circuits can be employed to well deduce the structure and various electrical parameters of the Cr(III) conversion coatings. Moreover, the structure of all the Cr(III)

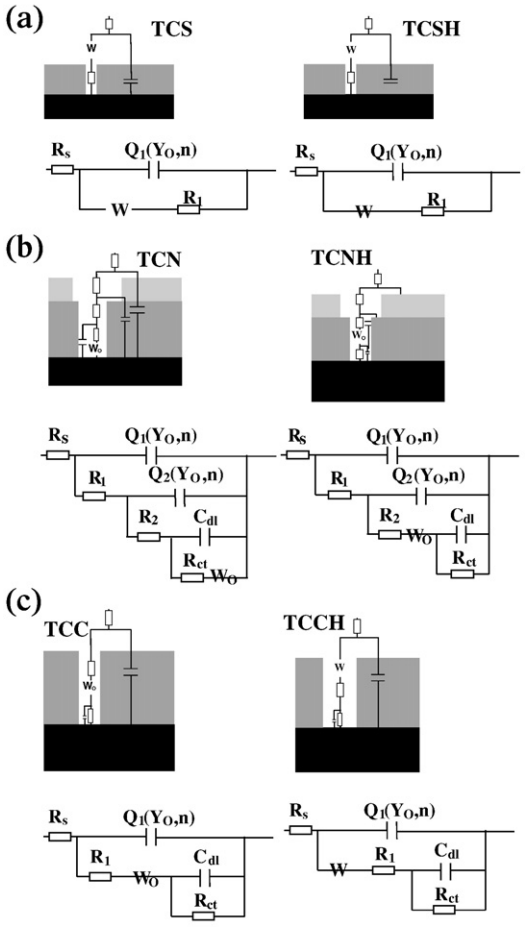

Fig. 7. Equivalent circuits of the Cr(III) conversion coatings: (a) TCS and TCSH, (b) TCN and TCNH, and (c) TCC and TCCH specimen.

Table 3
Various electrical parameters of the as-deposited and baked Cr(III) conversion coatings

	R_s	Q1		R_1	Q2		R_2	W	W_O		C_{dl}	R_{ct}	R_P
		$Y_0(C_1)$	n_1		$Y_0(C_2)$	n_1		Y_0	Y_0	B			
TCS	57.9	3.6	0.81	2.69 K				3646					2.69 K
TCSH	60.3	2.1	0.86	7.06 K				1062					7.06 K
TCN	52.5	0.21	0.63	17.05	4.35	0.97	2.95 K		330.7	2.71	194.6	1.51 K	4.47 K
TCNH	52.5	8.54	0.70	10.16	7.86	0.93	0.51 K		282.1	1.90	3.06	1.02 K	1.54 K
TCC	54.1	0.47	0.55	8.28					455.0	0.14	10.59	0.31 K	0.32 K
TCCH	56.6	9.17	0.78	24.49				86760			12.82	0.63 K	0.65 K

Note: (1) $R_p = R_1 + R_2 + R_{dl}$.
(2) units: R, R_{dl} (Ω cm^2); Y_0 ($\mu s^n\ \Omega^{-1}$ cm^{-2}); C, C_{dl} (μF/cm^2).

conversion coatings established by the EIS equivalent circuits is in agreement with those examined by SEM observations, as shown in Figs. 2 and 3.

4. Conclusions

Three Cr(III)-based solutions containing sulfate, nitrate, or chloride were used to fabricate conversion coatings on electrogalvanized steels. The OCP curves of these galvanized steels show that the ranking of the formation potential (ΔE) of the Cr(III) conversion coatings, from the large to the small, is as follows: TCN, TCC, and TCS. The formation time (Δt) of these coating is approximately 60 s–120 s. Equivalent circuits were constructed to reasonably assess the structure of the conversion coatings. The structure and corrosion resistance of the Cr(III) conversion coatings, before and after baking, can be evaluated by the combination of the EIS results and the SEM observations. The TCS and TCSH coatings display a dense one-layer structure, whereas, the TCN and TCNH coatings are composed of two porous layers. The TCC and TCCH coatings exhibit a porous single-layer structure. There is no apparent cracks observed in the conversion coatings, indicating that the internal stress is relatively small in the thin (TCS and TCSH) or porous (TCN, TCNH, TCC, and TCCH) coatings prepared under the conditions of this present study. Moreover, the difference in the coating structure and properties is evidently due to the various anions in the baths.

The OCP measurements, EIS analyses, and SEM observations have been employed for studying the formation procedures, structure, and characteristics of the Cr(III) conversion coatings formed in the various baths. To further study the properties of Cr(III) conversion coatings, the methods and results in this study can facilitate the selection of proper Cr(III) salts for the conversion coating treatment of electrogalvanized steels, and the structural identification of the Cr(III) conversion coatings.

References

[1] N.T. Wen, F.J. Chen, M.D. Ger, Y.N. Pan, C.S. Lin, Electrochem. Solid State Lett. 11 (2008) C47.
[2] R. Berger, U. Bexell, T.M. Grehk, S.E. Hörnström, Surf. Coat. Technol. 202 (2007) 391–397.
[3] I.M. Baghni, S.B. Lyon, B. Ding, Surf. Coat. Technol. 185 (2004) 194.
[4] K.W. Cho, V.S. Rao, H.S. Kwon, Electrochim. Acta 52 (2007) 4449.
[5] R. Ramanauskas, L. Gudaviciute, L. Diaz-Ballote, P. Bartolo-Perez, P. Quintana, Surf. Coat. Technol. 140 (2001) 109.
[6] X. Zhang, C. van den Bos, W.G. Sloof, A. Hovestad, H. Terryn, J.H.W. de Wit, Surf. Coat. Technol. 199 (2005) 92.
[7] F.X. Perrin, M.P. Gigandet, M. Wery, J. Pagetti, Surf. Coat. Technol. 105 (1998) 135.
[8] M.P. Gigandet, J. Faucheu, M. Tachez, Surf. Coat. Technol. 89 (1997) 285.
[9] Y.J. Tan, S. Bailey, B. Kinsella, Corros. Sci. 38 (1996) 1545.
[10] M.L. Zheludkevich, R. Serra, M.F. Montemor, K.A. Yasakau, I.M.M. Salvado, M.G.S. Ferreira, Electrochim. Acta 51 (2005) 208.
[11] H. Kaesche, Electrochim. Acta 9 (1964) 383.
[12] B.M. Rosales, H. Gerischer, J. Electrochem. Soc. 132 (1985) 1281.
[13] C. Barnes, J.J.B. Ward, T.S. Sehmbhi, V.E. Carter, Trans. Inst. Met. Fin. 60 (1982) 45.
[14] V. Barranco, S. Feliu, S. Feliu, Corros. Sci. 46 (2004) 2203.
[15] H. Duan, K. Du, C. Yan, F. Wang, Electrochim. Acta 51 (2006) 2898.
[16] T. Jacobsen, K. West, Electrochim. Acta 40 (1995) 255.
[17] T.K. Rout, Corros. Sci. 49 (2007) 794.
[18] L. Kouisni, M. Azzi, F. Dalard, S. Maximovitch, Surf. Coat. Technol. 192 (2005) 239.
[19] P. Campestrini, E.P.M. van Westing, J.H.W. de Wit, Electrochim. Acta 46 (2001) 2631.
[20] J.S. Park, J.H. Choi, J.J. Woo, S.H. Moon, J. Colloid Interface Sci. 300 (2006) 655.